PAIN

Inhibition of somatosensory mechanotransduction by annexin A6

Ramin Raouf[1]*[†], Stéphane Lolignier[1]*[‡], Jane E. Sexton[1]*, Queensta Millet[1], Sonia Santana-Varela[1], Anna Biller[1], Alice M. Fuller[1], Vanessa Pereira[1], Jyoti S. Choudhary[2], Mark O. Collins[3], Stephen E. Moss[4], Richard Lewis[5], Julie Tordo[6][§], Els Henckaerts[6], Michael Linden[6], John N. Wood[1][‖]

Mechanically activated, slowly adapting currents in sensory neurons have been linked to noxious mechanosensation. The conotoxin NMB-1 (noxious mechanosensation blocker-1) blocks such currents and inhibits mechanical pain. Using a biotinylated form of NMB-1 in mass spectrometry analysis, we identified 67 binding proteins in sensory neurons and a sensory neuron–derived cell line, of which the top candidate was annexin A6, a membrane-associated calcium-binding protein. Annexin A6–deficient mice showed increased sensitivity to mechanical stimuli. Sensory neurons from these mice showed increased activity of the cation channel Piezo2, which mediates a rapidly adapting mechano-gated current linked to proprioception and touch, and a decrease in mechanically activated, slowly adapting currents. Conversely, overexpression of annexin A6 in sensory neurons inhibited rapidly adapting currents that were partially mediated by Piezo2. Furthermore, overexpression of annexin A6 in sensory neurons attenuated mechanical pain in a mouse model of osteoarthritis, a disease in which mechanically evoked pain is particularly problematic. These data suggest that annexin A6 can be exploited to inhibit chronic mechanical pain.

INTRODUCTION

Pain is the greatest clinical challenge of the age in numerical terms, and mechanically evoked pain is a major issue in many pain states, particularly those linked to arthritis and musculoskeletal pain that occur more frequently in older people (*1*). A subset of primary nociceptive neurons is directly activated by mechanical stimuli (*2*). In these neurons, genes encoding mechanically gated ion channels are transcriptionally activated by nerve growth factor (NGF), and ion channel trafficking is potentiated by protein kinase C (*3*). Mechanical pain is enhanced by NGF or phorbol esters, suggesting that the mechanically activated (MA) currents identified in sensory neurons have a major role in mechanosensation (*3*). Mechanically gated currents in sensory neurons have been classified on the basis of their adaptation kinetics (*4*). Rapidly adapting (RA) currents have been linked to proprioception and touch through the activation of the mechanically gated ion channel Piezo2 (*5*, *6*). Deletion of Piezo2 with Advillin Cre-ER[T2] abolishes >80% of RA currents in sensory neurons, as well as 50% of intermediately adapting (IA) currents (*5*). Slowly adapting (SA) and IA channels have also been linked to noxious mechanotransduction (*7*).

Although Piezo2 contributes to mechanical allodynia through EPAC-mediated regulation (*8*), the principal mechanically gated ion channels responsible for noxious mechanosensation have yet to be identified. Some TRP channels, for example, TRPC3, seem to contribute to mechanosensory currents, although a contribution of endogenous Piezo channels is a potential confounding factor (*9*). An SA mechanosensitive channel, TMEM150c or TNN, expressed in muscle spindles and their afferents does not appear to have a role in mechanical pain (*10*). Potassium channels found in sensory neurons are also mechanosensors (*11*). Thus, at least four distinct channel subtypes (TRPs, TMEMs, Piezos, and K channels) may contribute to somatosensory mechanotransduction.

A screen for toxins that block mechanosensitive channels has identified NMB-1 (noxious mechanosensation blocker-1), a conotoxin peptide that selectively inhibits the persistent, nonadapting IA component and SA MA currents in sensory neurons (*7*). NMB-1 binds to small-diameter, peripherin-positive neurons (*7*), which are responsible for noxious mechanotransduction (*12*). NMB-1 also inhibits mechanotransduction currents in the cochlea and blocks behavioral responses to noxious mechanical stimuli. To identify the targets to which NMB-1 binds and therefore identify proteins that contribute to mechanotransduction, we developed a biotinylated form of NMB-1 that retained activity. Using sensory neurons and sensory neuron–derived cell lines, we performed immunoblotting and pull-down assays using biotinylated NMB-1 (bNMB-1) followed by mass spectrometry (MS) analysis. Several candidates were identified, including the Ca^{2+}-dependent, phospholipid-binding protein annexin A6. Here, we described a role for annexin A6 in mechanotransduction in sensory neurons and the implications of this role in blocking mechanical pain.

RESULTS

Identification of NMB-1–binding proteins shows that NMB-1 interacts with annexin A6

We have shown that bNMB-1 can specifically bind peripherin-positive dorsal root ganglion (DRG) neurons rather than large-diameter sensory

[1]Molecular Nociception Group, Wolfson Institute for Biomedical Research, University College London (UCL), Gower Street, London WC1E 6BT, UK. [2]Wellcome Genome Campus, Hinxton, Cambridge CB10 1SA, UK. [3]Department of Biomedical Science, The University of Sheffield, Western Bank, Sheffield S10 2TN, UK. [4]Institute of Ophthalmology, UCL, 11-43 Bath Street, London EC1V 9EL, UK. [5]Institute for Molecular Bioscience, University of Queensland, Brisbane, St. Lucia, Queensland 4072, Australia. [6]Department of Infectious Diseases, King's College London School of Medicine, London SE1 9RT, UK.
*These authors contributed equally to this work.
†Present address: Wolfson Centre for Age-Related Diseases, King's College London, London SE1 1UL, UK.
‡Present address: NEURO-DOL, UMR1107 INSERM/Université Clermont Auvergne, 63000 Clermont-Ferrand, France.
§Present address: Cell and Gene Therapy Catapult, Guy's Hospital, London SE1 9RT, UK.
‖Corresponding author. Email: j.wood@ucl.ac.uk

neurons. bNMB-1 retains its activity in blocking SA mechanically evoked currents in these neurons (*7*). We used this modified form of the toxin to identify proteins that interact with NMB-1 in rat DRG neurons. We developed an immunoblotting protocol to stain interacting proteins on Western blots of DRG or cerebellum membrane protein extracts and found that bNMB-1 can bind specific bands from DRG protein extracts, whereas the same pattern of staining was not present in protein extracts from the cerebellum (fig. S1A). Because of the low yield of protein recovery from polyvinylidene difluoride (PVDF) membrane strips, we identified binding proteins by juxtaposing alongside the blot an identically processed polyacrylamide gel stained with metallic silver to visualize all the proteins (fig. S1A). We used liquid chromatography–tandem MS (LC-MS/MS) analysis to identify peptides present in bands from the gel that corresponded to positions of bNMB-1–reactive bands on the blot (data file S1). To restrict this list of potential NMB-1–interacting partners to proteins associated with the mechanotransduction complex, we used a pull-down approach using the differentiated nociceptor cell line ND-C, a DRG neuron–derived cell line that shows discrete MA currents akin to DRG neurons in culture (*13, 14*). We performed a pull-down assay for NMB-1 from differentiated ND-C cell protein extracts (fig. S1B) and identified proteins present in the pull-downs using MS (table S1 and data file S2). We reasoned that the list of proteins from the intersection of the two tables would be the smallest set containing bNMB-1–interacting proteins and found that annexin A6 was the most abundant protein shared between the two lists (Table 1).

Annexin A6 is a calcium-dependent membrane-binding protein that is expressed by most sensory neurons. It has been suggested to modulate Ca^{2+} conductance in DRG neurons (*15*) and to mediate mechanotransduction currents in lipid bilayers. Incubation of wild-type (WT) and *Anxa6* knockout (KO) DRG tissue with bNMB-1 and fluorescently tagged avidin (fig. S2, A to F) revealed a substantial decrease in binding of bNMB-1 to *Anxa6* KO tissue (fig. S2G). The residual binding observed in *Anxa6* KO tissue also confirmed that NMB-1 bound not only annexin A6 complexes but also other membrane proteins in sensory neurons. We also confirmed that an immunoreactive annexin A6 band ran at the appropriate molecular weight to one of the bands selected for sequencing (protein band labeled "5" in fig. S1A) was present in the preparation that produced an annexin A6 signal on MS analysis (fig. S2A). On the basis of this evidence for an interaction between NMB-1 and annexin A6, we next examined the effects of annexin A6 on mechanotransduction in DRG neurons.

Annexin A6 deletion potentiates mechanical pain in mice and mechanosensory currents of sensory neurons

Using global *Anxa6* KO mice, we investigated the role of annexin A6 in mechanosensation in vivo. WT and *Anxa6* KO mice showed similar tactile thresholds, as assessed with the von Frey test (Fig. 1A). However, in response to noxious mechanical pressure, *Anxa6* KO mice showed a 17.5% decrease in the force required to elicit a response (Fig. 1B). These findings suggest that annexin A6 is involved in noxious, but not innocuous mechanosensation.

We then investigated mechanotransduction at the cellular level in cultured sensory neurons from WT and *Anxa6* KO mice DRGs by recording MA currents in whole-cell patch-clamp configuration (*2, 16*). Currents were evoked by applying focal pressure to the cell membrane with a polished glass pipette while cells were held at

−70 mV. Sensory neurons were either mechanically insensitive (nonresponding) or mechanically sensitive, with an MA current defined by its adaptation kinetics as RA, IA, or SA. Cell capacitance did not differ between WT and *Anxa6* KO neurons, whatever their response to mechanical stimulation (Fig. 2A). We observed a 1.8-fold decrease in the percentage of neurons displaying an SA current, mostly in favor of nonresponding neurons, which were increased 1.9-fold in the KO (Fig. 2B). The minimum stimulation required to elicit a >40-pA MA current was similar in WT and KO neurons, whatever the current kinetics (Fig. 2C). However, the maximum density of transient RA and IA currents when combined was 3.5-fold higher in *Anxa6* KO neurons compared to WT neurons. There was a 4.1-fold decrease in the maximum density of SA currents in *Anxa6* KO compared to WT neurons (Fig. 2D). When plotted against the displacement produced by the stimulation probe, these observations showed a substantial increase in RA and IA current density and a decrease in SA current density in *Anxa6* KO neurons compared to WT neurons (Fig. 2, E to H, and fig. S3, A and B). These data support a potential contribution of annexin A6 to the SA current.

We next assessed whether overexpressing annexin A6 in DRG neurons had the opposite effect on mechanotransduction to that induced by knocking out *Anxa6*. Cultured DRG neurons were transfected with a cytomegalovirus promoter (CMV)–driven expression vector containing variant 1 of human *ANXA6* together with the fluorescent protein tdTomato, or the corresponding empty vector. MA currents were recorded in tdTomato-positive neurons 2 days after transfection. Cell capacitance did not differ between cells transfected with *ANXA6* or empty vector, whatever their response to mechanical stimulation (Fig. 3A). Transfection did not alter the percentage of cells with the different types of MA current (Fig. 3B) or MA current thresholds (Fig. 3C), whatever the current kinetics. However, we observed a 2.63-fold decrease in the maximum RA and IA current density (Fig. 3D) in neurons transfected with the *ANXA6*-containing construct compared to those transfected with empty vector. An increase in the maximum SA MA current density recorded in neurons transfected with the *ANXA6*-containing construct was also observed, although this was not significant (Fig. 3D). The significant decrease in RA and IA current density can be seen in current density/displacement curves, whereas for SA currents, neurons transfected with the empty vector or with the *ANXA6* expression vector showed similar currents (Fig. 3, E to H, and fig. S3, C and D).

Therefore, annexin A6 inhibited transient MA currents in DRG neurons, as shown by the decrease in these currents in neurons overexpressing the human clone and by their enhancement in *Anxa6* KO DRG neurons. *Anxa6* deletion was linked to a loss of SA currents, suggesting a possible contribution of annexin A6 to SA mechanotransduction complexes. Gene deletion studies have shown that >80% of RA currents and 50% of intermediate adapting currents are lost in the absence of Piezo2 (*5*).Thus, annexin A6 has a functional link with this channel in sensory neurons. We therefore studied the effects of annexin A6 on MA currents produced by Piezo2 in a heterologous expression system to further explore this interaction.

Expression vectors containing the human *ANXA6* or *PIEZO2* clones [together with a tdTomato or green fluorescent protein (GFP), respectively], or their corresponding empty vectors, were cotransfected into ND-C cells (*14*). Membrane capacitance of recorded

Table 1. NMB-1–interacting candidates shared between DRG and ND-C cells. Mouse Uniprot numbers are given. Total matches refer to combined numbers of positive peptide matches for each candidate.

| Gene	Uniprot	Name	Molecular weight	Total matches
Anxa6	P14824	Annexin A6, calcium-dependent phospholipid binding	75,838	36
Flna	Q8BTM8	Filamin-A, actin binding	274,142	28
Myh9	A2VCK1	Myosin-9, actin filament binding	226,232	22
Vim	P20152	Vimentin, structural constituent of cytoskeleton	53,655	21
Anxa5	P48036	Annexin A5, calcium-dependent phospholipid binding	35,730	8
Hnrpu	O88568	Heterogenous nuclear ribonucleoprotein U, core promoter binding activity	87,863	8
Snd1	Q78PY7	Staphylococcal nuclease domain-containing protein 1 nuclease domain-containing protein 1, cadherin binding involved in cell-cell adhesion	102,025	7
Nono	Q99K48	Non-POU domain-containing octamer-binding protein, chromatin binding	54,506	6
L1cam	Q6PGJ3	Neural cell adhesion molecule L1, PDZ domain binding	140,969	5
Pdia6	Q3THH1	Protein disulfide-isomerase A6, protein disulfide isomerase activity, platelet activation	48,627	5
Anxa4	Q9R0V2	Annexin A4, calcium-dependent phospholipid binding	24,211	4
Cpsf6	Q6NVF9	Cleavage and polyadenylation specific factor 6, 68 kDa (predicted), isoform CRA_b, mRNA binding	59,116	4
Matr3	Q8K310	Matrin-3, nucleotide binding	94,572	3
Sfxn3	Q91V61	Sideroflexin-3, tricarboxylate secondary active transmembrane transporter activity	31,636	3
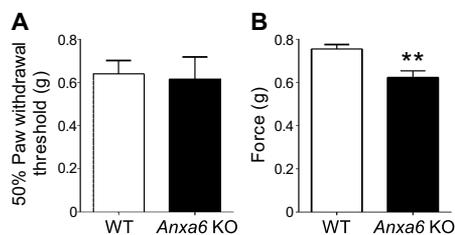
Fig. 1. Sensitivity of *Anxa6* KO mice to noxious mechanical stimuli. (**A**) Response to stimulation of the paw with von Frey hairs in WT and *Anxa6* KO mice. (**B**) Tail withdrawal threshold of WT and *Anxa6* KO mice in response to the application of a blunt probe. *n* = 9 WT and 8 KO mice. **$P < 0.01$ Student's unpaired *t* test.

cells was similar between the groups (Fig. 4A). Annexin A6 transfection alone did not affect the endogenous MA current threshold, maximum density, or current density/probe displacement relationship (Fig. 4, B to D). *Piezo2* alone produced a low-threshold RA current that is modulated by annexin A6. The mechanical threshold of this current increased 2.5-fold in cells transfected with *PIEZO2* alone compared to cells transfected with both *PIEZO2* and *ANXA6* (Fig. 4B). The maximum density of the Piezo2 current was also reduced by 2.8-fold with *ANXA6* coexpression (Fig. 4C), a decrease that was also significant on current density/displacement curves (Fig. 4D and fig. S3E). These data confirmed that the effects of annexin A6 on RA in DRG neurons are largely due to inhibition of Piezo2 mediated currents.
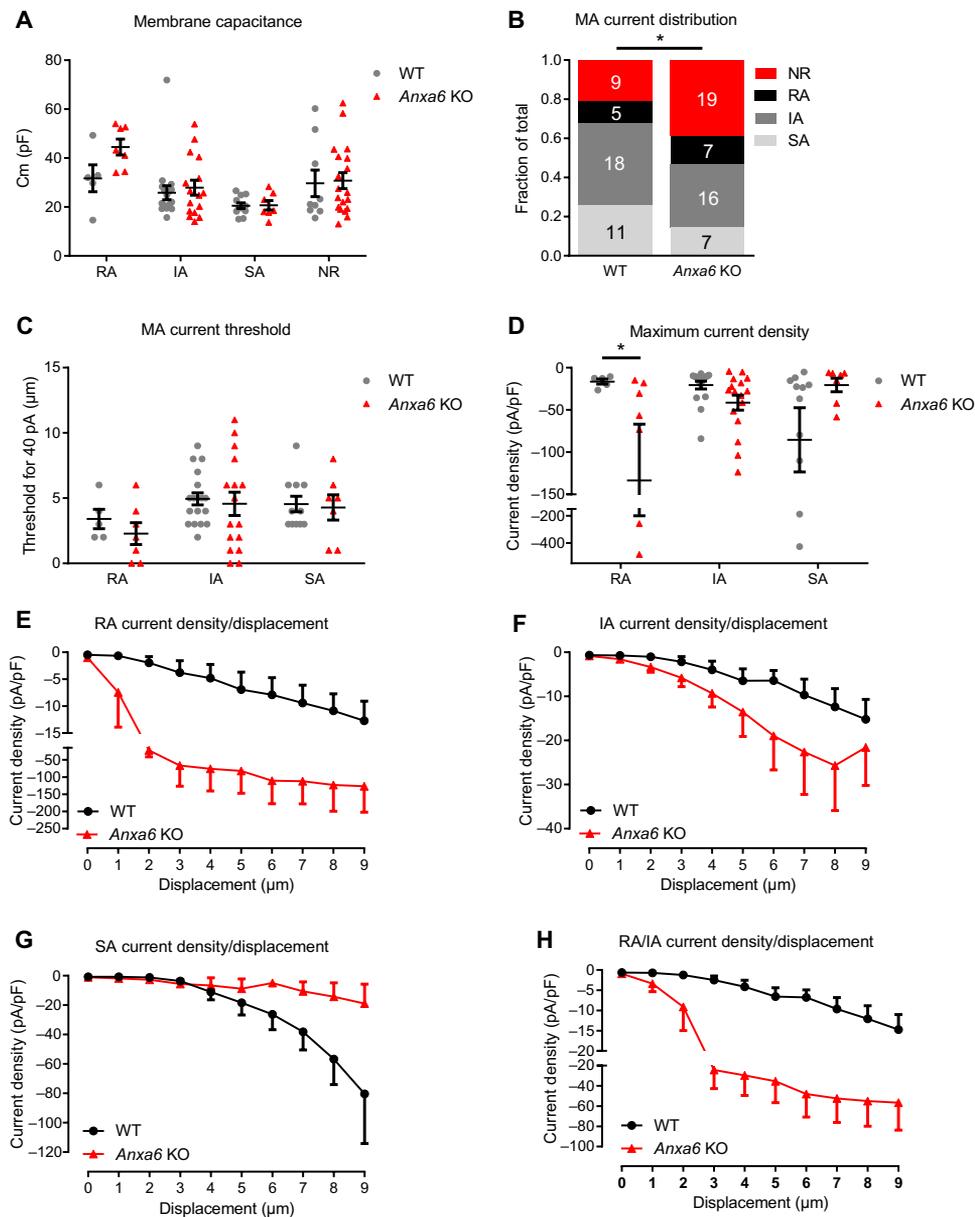
Fig. 2. Mechanotransduction in *Anxa6* KO sensory neurons. Mechanotransduction was assessed in cultured sensory neurons from WT and *Anxa6* KO DRGs. (**A**) Membrane capacitances of recorded WT and *Anxa6* KO neurons with RA, IA, or SA mechano-gated current and in nonresponsive (NR) neurons. Cm, membrane capacitance. (**B**) Distribution of the recorded neurons based on the MA current displayed. (**C**) Minimal stimulation intensity required to elicit a >40-pA MA current in WT and *Anxa6* KO neurons. (**D**) Maximum current density (Imax/Cm) recorded in WT and *Anxa6* KO neurons. (**E** to **H**) Current density plotted against the displacement of the mechanical probe for RA (E), IA (F), and SA (G) currents and the merged transient RA/IA currents (H). (A, C, and D) *$P < 0.05$, WT compared to *Anxa6* by two-way analysis of variance (ANOVA) followed by Fisher's least significant difference (LSD) multiple comparisons test. (B) *$P < 0.05$ by χ^2 test. (C) Two-way ANOVA followed by Sidak $P = 0.13$, 0.80, and 0.99 for RA, IA, and SA, respectively. (D) Two-way ANOVA followed by Sidak $P = 0.046$, 0.45, and 0.059 for RA, IA, and SA, respectively. (E to H) Two-way ANOVA $P = 0.002$, 0.0007, 0.0007, and <0.0001 for RA, IA, SA, and RA/IA, respectively. n values are given in (B) and represent the number of neurons.

In addition to annexin A6, we tested other identified peptide-binding partners of NMB-1 for a role in mechanosensation. ATP6V1B2 is the brain isoform of a vacuolar adenosine 5′-triphosphate (ATP) synthase subunit, which is expressed in cochlear hair cells and has

been linked to a role in hearing (*17*). However, expression of ATP6V1B2 in human embryonic kidney (HEK) 293T or ND-C cells did not produce an MA current (fig. S4, A to D), although co-expression of the subunit with *PIEZO2* partially reduced its peak amplitude similarly to annexin A6 (fig. S4, A and B).

Overexpression of *ANXA6* reduces mechanical pain in a mouse model of osteoarthritis

We extended our overexpression studies to a behavioral analysis of mechanosensation in a mouse model of osteoarthritis pain where mechanically evoked pain is particularly problematic. We generated AAV viruses (serotype TT) carrying the human *ANXA6* variant 1 clone upstream of an IRES-GFP construct and under the control of a CMV promoter. Although a sensory neuron–specific promoter would have been preferable for these studies, the size limitations on AAV inserts precluded this approach. AAV-TT carrying *ANXA6* or the empty control virus was delivered intrathecally to infect sensory neuron cell bodies, an approach that has been experimentally validated (*18*). We used GFP downstream of an IRES in the constructs to show that DRG neurons were effectively transduced by the virus.

Pain thresholds were followed for 12 weeks before a single dose of monosodium iodoacetate (MIA) was injected into the left knee, and behavioral assessment continued for another 3 weeks whereupon mice were sacrificed to confirm successful transduction of DRG neurons (fig. S5). AAV-mediated overexpression of *ANXA6* decreased noxious mechanical sensitivity without affecting thermal sensitivity (Fig. 5, A and B). The 50% paw withdrawal thresholds in response to von Frey filaments (*19*), a test that characterizes mechanical sensitivity, was similar in the two groups at week 12 (baseline before MIA injection; Fig. 5C). One week after injection of MIA, all treatment groups showed a significant decrease in 50% threshold compared to the threshold recorded at baseline (Fig. 5D). Control (AAV-TT-IRES-GFP–treated) mice showed a further 2.2-fold 55% drop in 50% threshold from 1 to 3 weeks post-MIA, whereas the 50% threshold of AAV-TT-*ANXA6*-IRES-GFP–treated mice dropped only by 1.13-fold 12% during this time period.
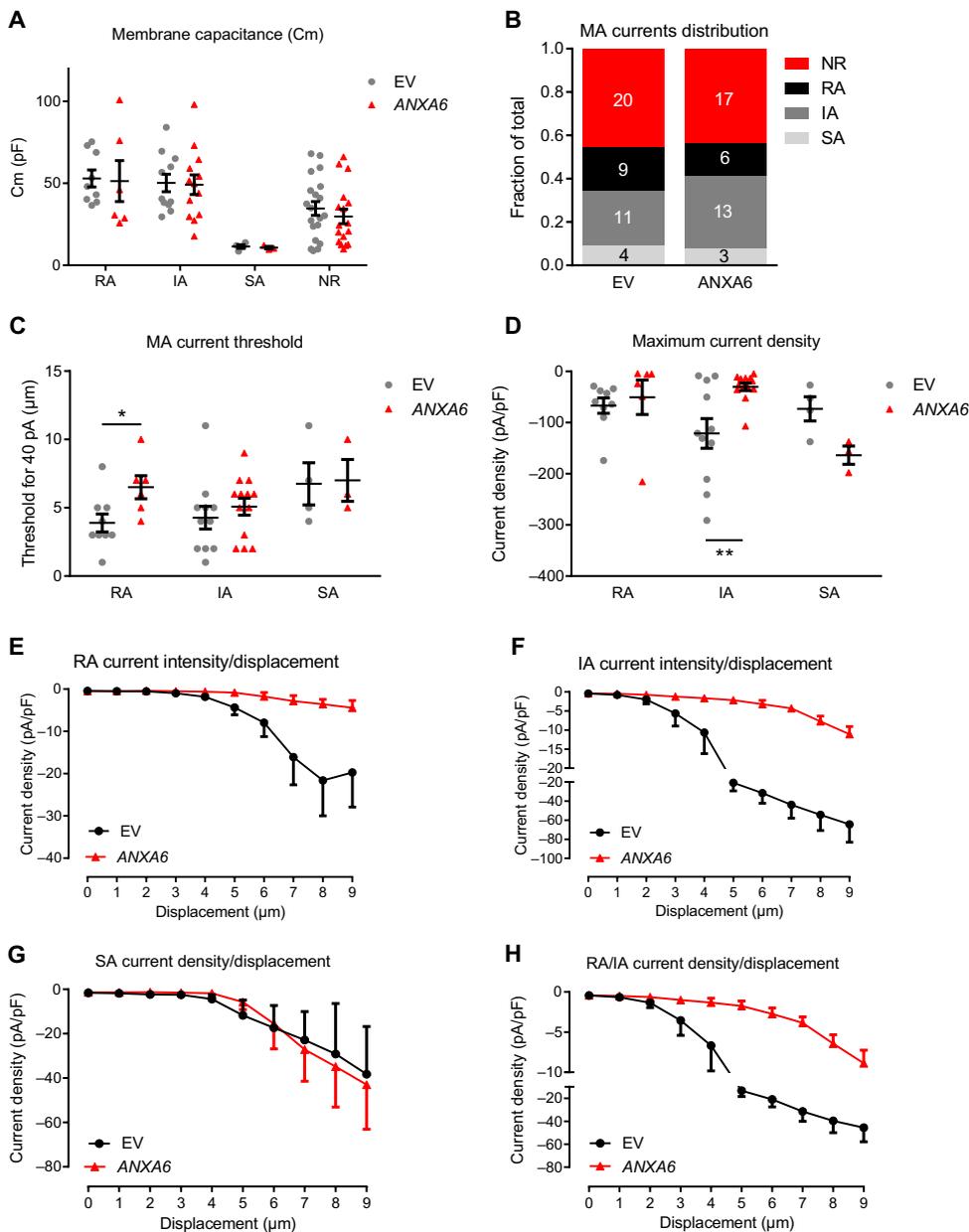
Fig. 3. Mechanotransduction in sensory neurons overexpressing *ANXA6*. Sensory neurons from WT mice were cultured and transfected with a human *ANXA6*-pIRES2-tdTomato construct or the corresponding pIRES2-tdTomato empty vector (EV). Only neurons expressing tdTomato were selected for mechano-clamp experiments. (**A**) Membrane capacitance of control and *ANXA6*-overexpressing neurons. (**B**) Distribution of the recorded neurons based on the MA current displayed. (**C**) Minimal stimulation intensity required to elicit a >40-pA MA current in control and *ANXA6*-overexpressing neurons. (**D**) Maximum current density (Imax/Cm) recorded in control and *Anxa6*-overexpressing neurons. (**E** to **H**) Current density plotted against the displacement of the mechanical probe for RA (E), IA (F), and SA (g) currents and merged transient RA/IA currents (H). (A, C, and D) *$P < 0.05$, **$P < 0.01$, EV compared to *ANXA6* by two-way ANOVA followed by Fisher's LSD multiple comparisons test. (B) χ^2 contingency test $P = 0.7452$. (E to H) Two-way ANOVA $P = 0.97$, 0.0004, <0.0001, and <0.0001 for SA, RA, IA, and RA/IA, respectively. *n* values are given in (B) and represent the number of neurons.

Mechanical hypersensitivity in AAV-TT-*ANXA6*-IRES-GFP–treated mice was also attenuated in the weight-bearing test, which evaluates mechanical pain by comparing the body weight applied on the MIA-injected paw over the total weight applied on both hind

paws. In control-treated mice, weight on the ipsilateral paw dropped by 1.15-fold 1 week after MIA injection and by 1.08-fold at 3 weeks. This asymmetry was significant compared to baseline at both time points, whereas *ANXA6*-treated mice did not develop a significant weight-bearing asymmetry at any time point. These results indicate that annexin A6 overexpression can prevent the onset of the weight-bearing asymmetry induced by MIA and suggest that gene therapy delivery of annexin A6 has potential use in treating human osteoarthritis pain by inhibiting mechanosensation in vivo.

DISCUSSION

The present studies demonstrated the ability of annexin A6 to modulate mechanotransduction in sensory neurons. Annexins are a superfamily of Ca^{2+}-dependent, phospholipid-binding proteins that are involved in diverse functional processes. They are highly evolutionarily conserved; annexin A6, previously known as p68, calelectrin, and protein III (*20*), is a compound gene that appears to derive from the evolutionarily early splicing of annexin A5 and annexin A10. Annexin A6 links the cellular cytoskeleton to the internal lipid bilayer of the cell membrane through calcium-dependent interactions with negatively charged phospholipids. We identified annexin A6 as a binding target of the biotinylated conotoxin NMB-1, which blocked behavioral responses to noxious mechanical stimuli and attenuated the persistent component of IA and SA MA currents. We hypothesized that annexin A6 would therefore be a potential candidate for a role in mechanotransduction. Annexin A6 has been suggested to form a cation-selective ion channel in lipid bilayers that is modulated by cGMP (guanosine 3′,5′-monophosphate) (*21*), or that low pH potentiates the ability of annexin A6 to form cation channels (*22*).

We found that annexin A6 KO mice had heightened sensitivity to noxious mechanical stimuli, and sensory neurons from these mice showed increased RA and IA mechanically evoked currents. Conversely, overexpressing annexin A6 reduced the RA current produced by the mechanotransduction channel Piezo2 in sensory neurons and heterologous expression systems. Intriguingly, loss of annexin A6 led to reduced SA currents. However, annexin A6 alone
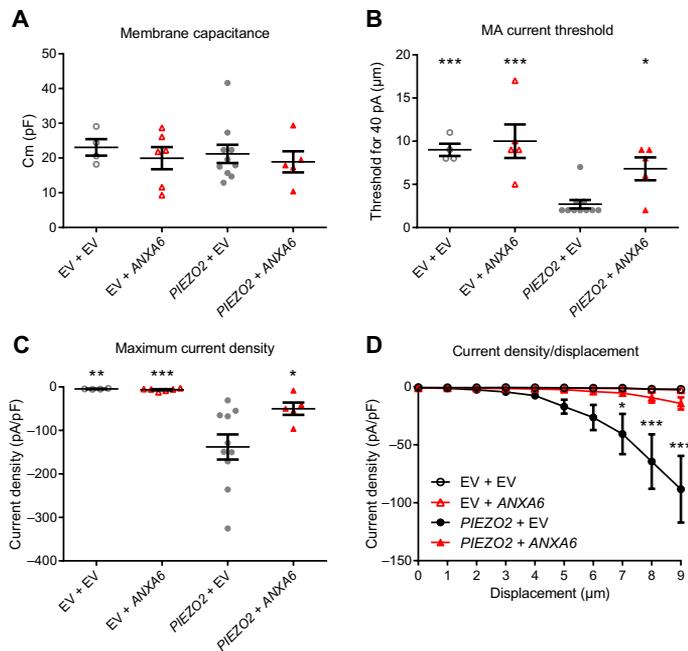
Fig. 4. Piezo2 MA current modulation by *ANXA6* coexpression. ND-C cells were cotransfected with *hPIEZO2*-IRES-eGFP and/or *hANXA6*-pIRES2-tdTomato or their respective EVs IRES-eGFP and pIRES2-tdTomato according to the indicated combinations, and mechanotransduction was assessed by the mechano-clamp technique. (**A**) Membrane capacitance of cells transfected as indicated. (**B**) Minimal stimulation intensity required to elicit a >40-pA MA current in cells transfected as indicated. (**C**) Maximum recoded MA current density in cells transfected as indicated. (**D**) Current density plotted against the displacement of the mechanical probe in cells transfected as indicated. (A to D) $*P < 0.05$, $**P < 0.01$, $***P < 0.001$ compared to *PIEZO2* + EV by one-way ANOVA followed by Fisher's LSD test (A to C) or two-way ANOVA followed by Fisher's LSD multiple comparisons test (D). $n = 4$ EV + EV, 6 EV + *ANXA6*, 10 *PIEZO2* + EV, and 5 *PIEZO2* + *ANXA6* cells.
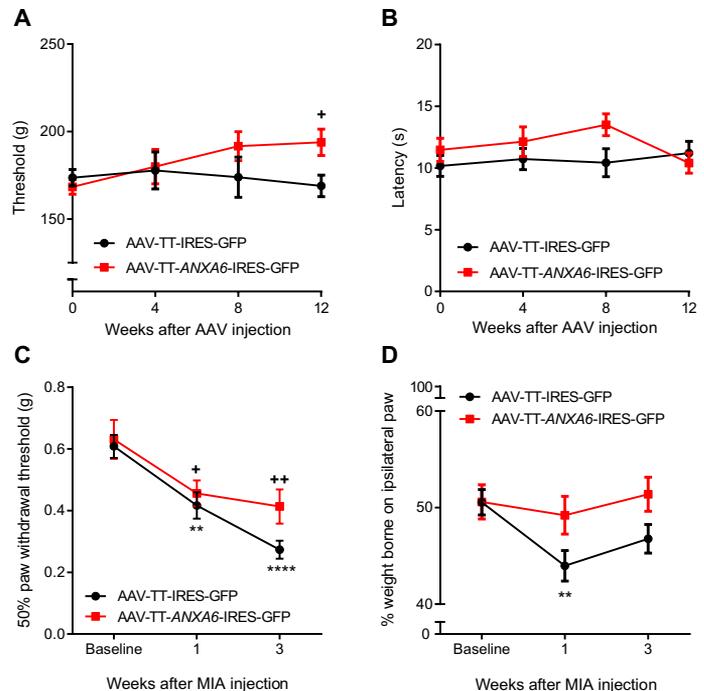

Fig. 5. Effect of virally mediated overexpression of *ANXA6* in sensory neurons on noxious mechanical sensitivity and mechanical hypersensitivity in the MIA model of osteoarthritis pain. WT mice received one intrathecal injection of AAV-TT viruses containing either a *hANXA6*-IRES-GFP construct or the IRES-GFP control. Pain thresholds were then monitored for 12 weeks, after which osteoarthritis was induced by a unilateral injection of MIA into the knee joint, and mechanical hypersensitivity was assessed for another 3 weeks. (**A**) Noxious mechanical sensitivity of mice injected with the indicated viruses and submitted to the paw pressure test. (**B**) Sensitivity to noxious heat of mice injected with the indicated viruses. (**C**) Mechanical hypersensitivity after unilateral osteoarthritis (OA) induction in mice injected with the indicated viruses. (**D**) Weight-bearing asymmetry as evaluated by the weight ratio between ipsilateral and contralateral rear paws in mice injected with the indicated viruses. Data are shown as mean ± SEM; two-way repeated-measures ANOVA with Dunnett's multiple comparison test; $**P < 0.01$, $****P < 0.001$ compared to 0 within AAV-TT-IRES-GFP; $^+P < 0.05$, $^{++}P < 0.01$ compared to 0 within AAV-TT-*ANXA6*-IRES-GFP; $n = 12$ mice per group.

does not encode a mechanosensitive current (Fig. 4D). It is thus nonetheless possible that annexin contributes to the complex that forms the SA channel in sensory neurons.

Annexin A6 inhibited RA and IA mechanotransduction currents, suggesting a possible role for annexin A6 in cutaneous mechanosensation. Annexin A6 has been linked to roles in mechanosensory functions in other physiological systems. For example, in mice overexpressing annexin A6 in cardiomyocytes, there is a decrease in their contractility, which is presumed to be the result of reduced free intracellular Ca^{2+} and reduced Ca^{2+} release upon depolarization (*23*). Similarly, in skeletal muscle, annexin A6 regulates the gating properties of the sarcoplasmic reticulum Ca^{2+} release channel, potentially linking it to a role in excitation-contraction coupling that mediates muscle contraction (*24*).

Current understanding of the functions of annexin A6 provides insight into the potential mechanisms by which it could regulate mechanotransduction. When Ca^{2+} is low, annexins are soluble monomeric proteins, although when intracellular Ca^{2+} levels rise, annexins can bind to phospholipid membranes (*15*). Membrane binding for annexins has been proposed to require the formation of trimers that aggregate into a hexagonal array surrounding a target protein (*15*, *25*, *26*). This aggregation affects membrane properties, for example, altering Ca^{2+}-mediated membrane fluidity (*27–30*) and

potentially interfering with protein-protein or protein-phospholipid interactions and affecting Ca^{2+}-dependent second messenger pathways (*31*). If annexin A6 can regulate membrane fluidity, increasing membrane rigidity in a similar way as annexin A5 for example (*30*), then it is possible that this could increase the force required to elicit an MA response. In this situation, it is possible that RA and IA currents, which are typically evoked by a lower intensity of mechanical displacement, would be most sensitive to changes produced by overexpressing annexin A6 in cells. This notion is consistent with the attenuation of RA and IA current amplitude in DRG neurons overexpressing annexin A6. Whether annexin A6 expression is regulated in sensory neurons in physiological conditions is currently unknown, but evidence from cardiomyocytes demonstrates the potential for its expression to be dynamically regulated in cells (*32*). Our gene therapy data suggest that annexin A6–mediated regulation of mechanosensation also has the potential to be clinically useful. Gene therapy offers a target-specific alternative to existing pharmacological interventions and is a viable treatment method for

analgesia in the clinic (33). Similarly, in preclinical models, gene therapy for pain relief is effective in multiple pain conditions (18, 34–37) including rheumatoid arthritis (38). We used an AAV serotype with a high tropism for sensory neurons, AAV-TT, to overexpress human *ANXA6* in vivo and found that overexpressing *ANXA6* attenuated mechanical hypersensitivity in the MIA model of osteoarthritis pain.

Other studies have identified proteins such as TRPC3, TRPC6, and TRPA1 as mechanosensors that function in a context-dependent manner (39, 40). Other proteins identified by NMB-1 peptide binding are now being examined for a possible role in mechanotransduction. The data presented suggest that annexin A6 may participate in the channel complex responsible for the SA mechanotransduction current that remains to be characterized. The present study also demonstrates an interesting role for annexin A6 in regulating mechanotransduction that may be clinically useful in terms of gene therapy.

MATERIALS AND METHODS
Ligand-blotting assay using DRG and cerebellum membrane protein extracts
Membrane proteins were isolated using a previously published protocol (41). Briefly, DRG (70 ganglia) and cerebellum were excised from P0 rats and homogenized using a glass Teflon homogenizer in homogenization buffer [0.32 M sucrose, 10 mM Hepes (pH 7.4), and 2 mM EDTA plus protease inhibitors leupeptin, pepstatin, phenylmethylsulfonyl fluoride, benzamidine, and aprotinin]. The homogenates were centrifuged for 15 min at $1000g$ and the supernatant was centrifuged at $200,000g$ for 15 min and extracted with lysis buffer [50 mM Hepes (pH 7.4), 2 mM EDTA, protease inhibitors, 4% SDS, and 2% Triton X-100]. The samples were resolved using SDS–polyacrylamide gel electrophoresis (PAGE) on 8 to 12% gels and transferred to PVDF or nitrocellulose filters (R&D Systems). The membrane was blocked with 0.1% Tween 20 in phosphate-buffered saline (PBST) (pH 7.4; wash buffer) and incubated with bNMB-1 (2 or 5 μM) for 15 min. The membranes were washed and treated with chilled 4% paraformaldehyde (PFA). This crosslinking step enhances the binding of NMB-1 (7). The membranes were incubated with alkaline phosphatase–conjugated streptavidin (Chemicon) for 2 hours at room temperature. bNMB-1 was detected using alkaline phosphatase color reaction using a BCIP/NBT (bromochloroindolyl phosphate–nitro blue tetrazolium) kit from Vector Laboratories according to the manufacturer's instructions. Levamisole solution (Vector Laboratories) was added to inhibit endogenous alkaline phosphatase activity. The appearance of blue precipitate was monitored on both bNMB-1–treated and control blots. Control experiments were also carried out where NMB-1 was substituted with goat anti-biotin immunoglobulin G (IgG) to ensure specificity of NMB-1 blotting assay. Reactive bands on the PVDF or nitrocellulose filters were cut and sent to Medical Research Council Clinical Sciences Centre (Imperial College London) for analysis. However, attempts to extract the proteins from the filter and process for LC-MS/MS or perform in situ digestion did not produce sufficient quantities of material required for mass spectroscopy. As an alternative approach, we split into two a mini-gel after resolving protein samples. One half was electrotransferred onto a nitrocellulose filter and processed for bNMB-1 binding, and the other half was silver-stained (Silver Stain Kit, Pierce, Thermo

Fisher Scientific). The silver-stained half was aligned with the bNMB-1 blot based on the protein markers' position and other landmarks. Gel bands corresponding to the position of the reactive bands on the blots were excised from the gel. The samples were analyzed using LC-MS/MS on an Agilent quadrupole time-of-flight LC/MS.

SDS-PAGE and Western blot using antibody recognizing annexin A6
The samples were resolved using SDS-PAGE on a 7.5% precast gel (Bio-Rad) and transferred to a PVDF membrane (Merck). The membrane was blocked with 5% Marvel in 1× PBST for 1 hour at room temperature and then incubated with an anti–annexin VI antibody (Abcam, ab31026) at a concentration of 1:500 at 4°C overnight. The membrane was washed in 1× PBST and then incubated with horseradish peroxidase–conjugated goat anti-rabbit IgG (Thermo Fisher Scientific) at a concentration of 1:1600 for 1 hour 30 min at room temperature. After further washing, the membrane was immersed in Pierce ECL Western Blotting substrate (Thermo Fisher Scientific) and then developed with an exposure time of 1 min.

NMB-1 pull-down from ND-C cell extracts
Seven 10-cm plates of subconfluent, actively dividing ND-C cells were treated for 3 days with Dulbecco's modified Eagle's medium (DMEM) containing 1 mM dibromo–cAMP (adenosine 3′,5′-monophosphate) and 0.2% fetal bovine serum (FBS). The cultures were incubated with 5 μM bNMB-1 for 3.5 min and fixed with chilled 4% PFA for 10 min. The extraction buffer containing protease inhibitors, 0.1% SDS, and 1% Triton X-100 was added directly to the plate. The cells were scraped and extracted for 3 hours on ice. The protein extract was vortexed, spun down, and incubated with prepared Neuroavidin gel matrix (Thermo Fisher Scientific) overnight at 4°C. The beads were washed three times, and the bound proteins were eluted according to the manufacturer's instructions by heating to 95°C for 10 min in 2 or 5% β-mercaptoethanol. Control samples were processed as above omitting bNMB-1.

LC-MS/MS analysis of NMB-1–binding proteins
Eluates from NMB-1 pull-down experiments were separated by SDS-PAGE using a NuPAGE 4 to 12% bis-tris gel (1.5 mm × 10 well, Invitrogen) using Mops buffer. The gel was stained overnight with colloidal Coomassie blue (Sigma-Aldrich). Each lane was excised into 16 bands that were cut into 1- to 2-mm cubes and in-gel–digested overnight using trypsin (sequencing grade; Roche). Peptides were extracted from gel bands twice with 50% acetonitrile/0.5% formic acid and dried in a SpeedVac (Thermo Fisher Scientific). Peptides were resuspended using 0.5% formic acid and were analyzed online using an Ultimate 3000 Nano/Capillary LC System (Dionex) coupled to an LTQ FT hybrid mass spectrometer (Thermo Electron) equipped with a nanospray ion source. Peptides were desalted online using a micro-precolumn cartridge (C18 Pepmap 100, LC Packings) and then separated using a 30-min reversed phase gradient (4 to 32% acetonitrile/0.1% formic acid) on a BEH C18 analytical column (235 μm internal diameter × 10 cm) (Waters).

The mass spectrometer was operated in standard data-dependent acquisition mode controlled by Xcalibur 2.0. The instrument was operated with a cycle of one MS (in the Fourier-transform ion cyclotron resonance cell) acquired at a resolution of 100,000 at m/z 400, with the top five most abundant multiply-charged ions in a given

chromatographic window subjected to MS/MS fragmentation in the linear ion trap. All data were processed using BioWorks V3.3 (Thermo Electron) and searched using Mascot server 2.2 (Matrix Science) against a mouse International Protein Index (IPI) sequence database (June 2007) using following search parameters: trypsin with a maximum of 2 miscleavages, 20 ppm for MS mass tolerance, 0.5 Da for MS/MS mass tolerance, with three variable modifications of acetyl (protein N term), carbamidomethyl (C), and oxidation (M). False discovery rates determined by reverse database searches and empirical analyses of the distributions of mass deviation and Mascot ion scores were used to establish score and mass accuracy filters. Application of these filters to this data set resulted in a <1% false discovery rate as assessed by reverse database searching. Protein hits from all data sets were BLAST-clustered using a threshold of 95% sequence homology over at least 50% of sequence length.

Proteomics data processing

All data were processed using BioWorks V3.3 (Thermo Electron) and searched using Mascot server 2.2 (Matrix Science) against a mouse IPI sequence database (June 2007) using following search parameters: trypsin with a maximum of two miscleavages, 20 ppm for MS mass tolerance, 0.5 Da for MS/MS mass tolerance, with three variable modifications of acetyl (protein N term), carbamidomethyl (C), and oxidation (M). False discovery rates determined by reverse database searches and empirical analyses of the distributions of mass deviation and Mascot ion scores were used to establish score and mass accuracy filters. Application of these filters to this data set resulted in a <1% false discovery rate as assessed by reverse database searching. Protein hits from all data sets were BLAST-clustered using a threshold of 95% sequence homology over at least 50% of sequence length.

Animals

All experiments were approved by the UK Home Office and performed under a Home Office project licence (PPL 70/7382). Seven- to eight-week-old male C57Bl6/J mice, Anxa6 KOs, or WT littermates were used and kept under 12/12 light cycle with food and water ad libitum. Anxa6 global KOs were previously generated by disruption of exon 3 with insertion of a neo cassette (42). Experimenters were blind to the genotype or treatment of the animals. AAV viruses were injected intrathecally [10 µl at 2.4×10^{12} viral particles (VP)/ml] 20 min after intravenous injection of mannitol (200 µl at 25%) to potentiate sensory neuron transduction (43). Osteoarthritis was induced by injection of 0.5 mg of MIA (Sigma-Aldrich) into the right knee joint cavity under light isoflurane anesthesia (44).

Plasmids

hANXA6 transcript variant 1 clone (NP_001146) was purchased from Origene (catalog no. RC202086) and subcloned into a pIRES2-tdTomato vector, originally made from a pIRES2-AcGFP1 backbone. hPIEZO2 (NP_071351 with single-nucleotide polymorphisms rs7234309 and rs3748428) was cloned into an IRES-eGFP vector as previously described (8).

AAV-TT virus production and purification

HEK293T cells were cotransfected with a pAAV-CMV-hANXA6-IRES-GFP plasmid containing the hANXA6 transcript variant 1 clone (NP_001146) upstream a GFP, flanked by the inverted terminal repeat sequences of AAV2, together with a helper plasmid providing the rep and AAV-TT cap genes in trans (45). Seventy-two hours after cotransfection with PEI-max (Polysciences, 3.5 ml PEI-max: 1 mg of DNA), cells were harvested by centrifugation and lysed by four freeze-thaw cycles (from −80° to 37°C) in lysis buffer [150 mM NaCl, 50 mM Tris (pH 8.5)] before benzonase treatment (5000 U/cell factory 10 chamber, corresponding to 6320-cm^2 growth area, 37°C for 30 min). Lysates were cleared by centrifugation and filtered at 0.22 µm. Cell culture supernatant was also harvested and precipitated by the addition of ammonium sulfate to 31.3%. The resulting pellet was also resuspended in lysis buffer, treated with benzonase, clarified by centrifugation, and filtered.

Recombinant AAV-TT virions were purified by fast protein liquid chromatography (ÄKTApurifier system, GE Healthcare) and an AVB sepharose affinity column [buffer A, PBS (pH 8); buffer B, 0.5 M glycine (pH 2.7)]. The collected fractions were then dialyzed against PBS overnight, and viruses were concentrated with Vivaspin 20 centrifugal concentrators (100 kDa MWCO, Sartorius). Viral genome and capside titers were determined by real-time quantitative polymerase chain reaction (PCR) and SDS-PAGE, respectively. Primers used for PCR quantification were the following: GFP, 5′-GACGGCAACATCCTGGGGCACAAG-3′ (forward) and 5′-CGGCGGCGGTCACGAACTC-3′ (reverse). A standard curve was generated by loading known quantities of the linearized pAAV-CMV-ANXA6-IRES-GFP vector plasmid. The vectors were finally diluted to 2.4×10^{12} VP/ml in saline before injection.

Behavior

Tactile sensitivity of the plantar surface of the animals was measured using the up-down method for obtaining 50% threshold using von Frey hairs (19). Animals were habituated to the von Frey chambers for 2 hours before the experiment. Noxious mechanical sensitivity was assessed using the Randall Selitto apparatus. Briefly, a blunt probe was applied to the tail with increasing force, and the force at which the animal withdrew was recorded (46). The test was performed three times for each animal.

Animals' weight distribution was assessed using an incapacitance meter (Linton Instrumentation). Mice were placed in the rearing position, with the upper body in a cylindrical chamber. The average weight applied by each hindpaw on the two sensors was measured over a 5-s period of steady behavior with both paws in contact with the sensors. Ipsilateral/contralateral weight ratios were calculated from three averaged consecutive measurements.

Immunohistochemistry

DRG and spinal cord were taken from mice after intracardiac perfusion with 4% PFA, postfixed for 2 hours in 4% PFA, and cryoprotected overnight in 30% sucrose (all solutions made from PBS). Tissues were embedded in optimal cutting temperature (OCT) compound and stored at −20°C until 10- and 30-µm cryosections of DRGs and spinal cord, respectively, were performed and mounted onto Superfrost Plus slides (Thermo Fisher Scientific). Slides were dried for 2 hours, blocked in 10% goat serum, and incubated overnight with a primary antibody anti-GFP (Abcam, #ab290, 1:2000), anti-ANXA6 (Abcam, #ab31026, 1/400), and/or with biotin-conjugated IB4 (Sigma-Aldrich, #L2140, 1:500). Slides were then incubated 2 hours with Alexa Fluor 488–conjugated goat anti-rabbit IgG (Abcam, #ab150077, 1:1000) and Alexa Fluor 568–streptavidin conjugate (Life Technologies, #S-11226, 1:1000). For NMB-1/annexin A6 interaction studies, lumbar DRG tissue was extracted

from three mice per genotype and snap-frozen on dry ice in OCT before being stored at −80°C. Sections were prepared as described above before being incubated in ice-cold 4% PFA for 8 min. Samples were blocked with protein block (Abcam, #64226) for 2 hours at room temperature before being incubated with 2 μM bNMB-1 (or no NMB-1 as control) in protein block overnight at 4°C. Samples were then treated with fluorescein isothiocyanate–conjugated avidin (Invitrogen, #434411; 1:1000) at room temperature for 2 hours. Images were taken on a Leica SP8 confocal microscope. Fluorescence was quantified in 6 to 10 sections per mouse using ImageJ software and normalized to background fluorescence.

Culture and transfection of DRG neurons

Immediately after CO_2 euthanasia, thoracic and lumbar DRGs were removed from 6- to 12-week-old mice and subsequently digested for 35 min at 37°C in Ca^{2+}- and Mg^{2+}-free Hanks' balanced salt solution containing 5 mM Hepes, 10 mM glucose, collagenase type XI (5 mg/ml), and dispase (10 mg/ml). After digestion, ganglia were gently triturated in DMEM containing 10% qualified FBS using fire-polished glass Pasteur pipettes. When required, neurons were electroporated using the Neon Transfection System (Life Technologies) according to the supplier's recommendations, in 10-μl tips and with 0.6 μg of plasmid per reaction, applying 2 × 20 ms pulses of 1100 V. Cells were plated on poly-L-lysine and laminin-coated dishes, in DMEM containing 10% FBS and 7S NGF (125 ng/ml). Neurons were kept at 37°C in 5% CO_2 and used for patch-clamp studies the following 2 days or at 48 ± 4 hours for electroporated neurons.

Culture and transfection of ND-C cells

ND-C cells, a hybridoma between neonatal rat DRG neurons and mouse neuroblastoma (*13*), were cultured in DMEM containing 10% FBS and kept at 37°C in 5% CO_2. Two days before patch-clamp recordings, the cells were electroporated using the Neon Transfection System according to the supplier's recommendations, in 10-μl tips and with 0.6 μg of plasmid per reaction, applying 3 × 20 ms pulses of 1100 V.

Electrophysiological recordings

Small (<30 pF) or large (>30 pF) DRG neurons whose somata were not in contact with those of other neurons, and who were displaying clear fluorescent signal when transfection was performed, were selected for electrophysiological recordings. Patch pipettes were pulled from borosilicate glass capillaries using a PC-10 puller (Narishige Group) and had a resistance of 1.5 to 3.5 megohms. The pipette solution contained 125 mM CsCl, 4.8 mM $CaCl_2$, 1 mM $MgCl_2$, 4 mM MgATP, 0.4 mM Na_2GTP, 10 mM EGTA, and 10 mM Hepes (pH 7.4 adjusted with CsOH; osmolarity, 310 mosm adjusted with sucrose). The bath solution contained 132 mM NaCl, 3 mM KCl, 2.5 mM $CaCl_2$, 1 mM $MgCl_2$, 10 mM glucose, and 10 mM Hepes (pH 7.4 adjusted with NaOH; osmolarity, 310 mosm adjusted with sucrose). Voltage- and current-clamp recordings were performed using a MultiClamp 200B amplifier and an Axon Digidata 1440A digitizer (Molecular Devices). Data were recorded and stored using Clampex 10 (Molecular Devices). Recordings were low-pass-filtered at 5 kHz and sampled at 20 kHz. Capacity transients were cancelled; however, series resistances were not compensated. Voltages were not corrected for junction potentials, and recordings were performed at room temperature. Holding command was set at −70 mV before and during mechanical stimulation. When required, membrane potential measurements were performed immediately after achieving whole-cell configuration. Offline analysis and fits were performed using Clampfit 10 (Axon Instruments, Molecular Devices).

Mechanosensory current analysis

Mechanical stimulation of cell bodies was achieved using a heat-polished glass pipette (tip diameter of about 2 μm) controlled by a piezoelectric crystal drive (Burleigh LSS-3000) and placed above the center of the cell soma at an angle of 70° to the surface of the dish. The probe was positioned so that a 10-μm movement did not visibly contact the cell but that an 11-μm movement, considered as a 1-μm stimulus, produced an observable membrane deflection. The probe was moved at a speed of 1 μm/ms. Mechanical steps (250 ms) were applied every 10 s in 1-μm increments. Currents were characterized as a function of the signal given by the highest stimulation intensity applied before the seal was lost. Cells were considered as nonresponding when no current >20 pA was observed in response to a 12-μm stimulus. Responding cells were then classified with regard to the adaptation kinetics of their currents. RA MA currents had a decay kinetics that was best described by a biexponential fit. IA MA currents had a decay kinetics that was best described by a monoexponential fit. SA currents showed minimal decay (<20%) during the 250-ms stimulation.

Data analysis

Raw data were analyzed for statistical significance using either unpaired Student's *t* test or one-way or two-way ANOVA with repeated measures, as appropriate, followed by Dunnett's multiple comparison test, Fisher's LSD multiple comparisons test, or χ^2 contingency test as indicated. Analysis was performed using GraphPad Prism 6 software. All values are shown as mean ± SEM.

SUPPLEMENTARY MATERIALS

www.sciencesignaling.org/cgi/content/full/11/535/eaao2060/DC1
Fig. S1. Isolation of NMB-1 peptide-binding partners.
Fig. S2. Interaction between NMB-1 and annexin A6.
Fig. S3. Representative traces of MA currents in vitro.
Fig. S4. ATP6V1B2 does not confer mechanosensitivity to HEK or ND-C cells but inhibits Piezo2 current.
Fig. S5. Transduction of DRG neurons using AAV-TT serotype.
Table S1. Top NMB-1–binding candidates in ND-C cells.
Data file S1. NMB-1–binding candidates in DRG neurons.
Data file S2. NMB-1–binding candidates from differentiated ND-C cells.

REFERENCES AND NOTES

1. R. L. Nahin, Estimates of pain prevalence and severity in adults: United States, 2012. *J. Pain* **16**, 769–780 (2015).
2. G. C. McCarter, D. B. Reichling, J. D. Levine, Mechanical transduction by rat dorsal root ganglion neurons in vitro. *Neurosci. Lett.* **273**, 179–182 (1999).
3. A. Di Castro, L. J. Drew, J. N. Wood, P. Cesare, Modulation of sensory neuron mechanotransduction by PKC- and nerve growth factor-dependent pathways. *Proc. Natl. Acad. Sci. U.S.A.* **103**, 4699–4704 (2006).
4. L. J. Drew, J. N. Wood, P. Cesare, Distinct mechanosensitive properties of capsaicin-sensitive and -insensitive sensory neurons. *J. Neurosci.* **22**, RC228 (2002).
5. S. S. Ranade, S.-H. Woo, A. E. Dubin, R. A. Moshourab, C. Wetzel, M. Petrus, J. Mathur, V. Bégay, B. Coste, J. Mainquist, A. J. Wilson, A. G. Francisco, K. Reddy, Z. Qiu, J. N. Wood, G. R. Lewin, A. Patapoutian, Piezo2 is the major transducer of mechanical forces for touch sensation in mice. *Nature* **516**, 121–125 (2014).
6. S.-H. Woo, S. Ranade, A. D. Weyer, A. E. Dubin, Y. Baba, Z. Qiu, M. Petrus, T. Miyamoto, K. Reddy, E. A. Lumpkin, C. L. Stucky, A. Patapoutian, Piezo2 is required for Merkel-cell mechanotransduction. *Nature* **509**, 622–626 (2014).
7. L. J. Drew, F. Rugiero, P. Cesare, J. E. Gale, B. Abrahamsen, S. Bowden, S. Heinzmann, A. Robinson, A. Brust, B. Colless, R. J. Lewis, J. N. Wood, High-threshold mechanosensitive ion channels blocked by a novel conopeptide mediate pressure-evoked pain. *PLOS ONE* **2**, e515 (2007).

8. N. Eijkelkamp, J. E. Linley, J. M. Torres, L. Bee, A. H. Dickenson, M. Gringhuis, M. S. Minett, G. S. Hong, E. Lee, U. Oh, Y. Ishikawa, F. J. Zwartkuis, J. J. Cox, J. N. Wood, A role for Piezo2 in EPAC1-dependent mechanical allodynia. *Nat. Commun.* **4**, 1682 (2013).

9. A. E. Dubin, S. E. Murthy, A. H. Lewis, L. Brosse, S. M. Cahalan, J. Grandl, B. Coste, A. Patapoutian, Endogenous Piezo1 can confound mechanically activated channel identification and characterization. *Neuron* **94**, 266–270.e3 (2017).

10. G. S. Hong, B. Lee, J. Wee, H. Chun, H. Kim, J. Jung, J. Y. Cha, T. R. Riew, G. H. Kim, I. B. Kim, U. Oh, Tentonin 3/TMEM150c confers distinct mechanosensitive currents in dorsal-root ganglion neurons with proprioceptive function. *Neuron* **91**, 107–118 (2016).

11. J. Noël, K. Zimmermann, J. Busserolles, E. Deval, A. Alloui, S. Diochot, N. Guy, M. Borsotto, P. Reeh, A. Eschalier, M. Lazdunski, The mechano-activated K+ channels TRAAK and TREK-1 control both warm and cold perception. *EMBO J.* **28**, 1308–1318 (2009).

12. B. Abrahamsen, J. Zhao, C. O. Asante, C. M. Cendan, S. Marsh, J. P. Martinez-Barbera, M. A. Nassar, A. H. Dickenson, J. N. Wood, The cell and molecular basis of mechanical, cold, and inflammatory pain. *Science* **321**, 702–705 (2008).

13. J. N. Wood, S. J. Bevan, P. R. Coote, P. M. Dunn, A. Harmar, P. Hogan, D. S. Latchman, C. Morrison, G. Rougon, M. Theveniau, S. Wheatley, Novel cell lines display properties of nociceptive sensory neurons. *Proc. Biol. Sci.* **241**, 187–194 (1990).

14. F. Rugiero, J. N. Wood, The mechanosensitive cell line ND-C does not express functional thermoTRP channels. *Neuropharmacology* **56**, 1138–1146 (2009).

15. J. M. Naciff, M. M. Behbehani, M. A. Kaetzel, J. R. Dedman, Annexin VI modulates Ca2+ and K+ conductances of spinal cord and dorsal root ganglion neurons. *Am. J. Physiol.* **271**, C2004–C2015 (1996).

16. P. Delmas, J. Hao, L. Rodat-Despoix, Molecular mechanisms of mechanotransduction in mammalian sensory neurons. *Nat. Rev. Neurosci.* **12**, 139–153 (2011).

17. Y. Yuan, J. Zhang, Q. Chang, J. Zeng, F. Xin, J. Wang, Q. Zhu, J. Wu, J. Lu, W. Guo, X. Yan, H. Jiang, B. Zhou, Q. Li, X. Gao, H. Yuan, S. Yang, D. Han, Z. Mao, P. Chen, X. Lin, P. Dai, De novo mutation in ATP6V1B2 impairs lysosome acidification and causes dominant deafness-onychodystrophy syndrome. *Cell Res.* **24**, 1370–1373 (2014).

18. A. M. Tan, O. A. Samad, S. D. Dib-Hajj, S. G. Waxman, Virus-mediated knockdown of Nav1.3 in dorsal root ganglia of STZ-induced diabetic rats alleviates tactile allodynia. *Mol. Med.* **21**, 544–552 (2015).

19. S. R. Chaplan, F. W. Bach, J. W. Pogrel, J. M. Chung, T. L. Yaksh, Quantitative assessment of tactile allodynia in the rat paw. *J. Neurosci. Methods* **53**, 55–63 (1994).

20. S. E. Moss, S. M. Jacob, A. A. Davies, M. J. Crumpton, A growth-dependent post-translational modification of annexin VI. *Biochim. Biophys. Acta* **1160**, 120–126 (1992).

21. A. Kirilenko, M. Golczak, S. Pikula, R. Buchet, J. Bandorowicz-Pikula, GTP-induced membrane binding and ion channel activity of annexin VI: Is annexin VI a GTP biosensor? *Biophys. J.* **82**, 2737–2745 (2002).

22. J. I. Kourie, H. B. Wood, Biophysical and molecular properties of annexin-formed channels. *Prog. Biophys. Mol. Biol.* **73**, 91–134 (2000).

23. A. M. Gunteski-Hamblin, G. Song, R. A. Walsh, M. Frenzke, G. P. Boivin, G. W. Dorn II, M. A. Kaetzel, N. D. Horseman, J. R. Dedman, Annexin VI overexpression targeted to heart alters cardiomyocyte function in transgenic mice. *Am. J. Physiol.* **270**, H1091–H1100 (1996).

24. M. Díaz-Muñoz, S. L. Hamilton, M. A. Kaetzel, P. Hazarika, J. R. Dedman, Modulation of Ca^{2+} release channel activity from sarcoplasmic reticulum by annexin VI (67-kDa calcimedin). *J. Biol. Chem.* **265**, 15894–15899 (1990).

25. N. O. Concha, J. F. Head, M. A. Kaetzel, J. R. Dedman, B. A. Seaton, Rat annexin V crystal structure: Ca(2+)-induced conformational changes. *Science* **261**, 1321–1324 (1993).

26. D. Voges, R. Berendes, A. Burger, P. Demange, W. Baumeister, R. K. Huber, Three-dimensional structure of membrane-bound annexin V. A correlative electron microscopy–X-ray crystallography study. *J. Mol. Biol.* **238**, 199–213 (1994).

27. A. Sobota, J. Bandorowicz, A. Jezierski, A. F. Sikorski, The effect of annexin IV and VI on the fluidity of phosphatidylserine/phosphatidylcholine bilayers studied with the use of 5-deoxylstearate spin label. *FEBS Lett.* **315**, 178–182 (1993).

28. M. Junker, C. E. Creutz, Endonexin (annexin IV)-mediated lateral segregation of phosphatidylglycerol in phosphatidylglycerol/phosphatidylcholine membranes. *Biochemistry* **32**, 9968–9974 (1993).

29. R. Newman, A. Tucker, C. Ferguson, D. Tsernoglou, K. Leonard, M. J. Crumpton, Crystallization of p68 on lipid monolayers and as three-dimensional single crystals. *J. Mol. Biol.* **206**, 213–219 (1989).

30. F. M. Megli, M. Selvaggi, S. Liemann, E. Quagliariello, R. Huber, The calcium-dependent binding of annexin V to phospholipid vesicles influences the bilayer inner fluidity gradient. *Biochemistry* **37**, 10540–10546 (1998).

31. M. A. Kaetzel, H. C. Chan, W. P. Dubinsky, J. R. Dedman, D. J. Nelson, A role for annexin IV in epithelial cell function. Inhibition of calcium-activated chloride conductance. *J. Biol. Chem.* **269**, 5297–5302 (1994).

32. P. Banerjee, V. Chander, A. Bandyopadhyay, Balancing functions of annexin A6 maintain equilibrium between hypertrophy and apoptosis in cardiomyocytes. *Cell Death Dis.* **6**, e1873 (2015).

33. D. J. Fink, J. Wechuck, M. Mata, J. C. Glorioso, J. Goss, D. Krisky, D. Wolfe, Gene therapy for pain: Results of a phase I clinical trial. *Ann. Neurol.* **70**, 207–212 (2011).

34. F.-f. Meng, Y. Xu, Q.-q. Dan, L. Wei, Y.-j. Deng, J. Liu, M. He, W. Liu, Q.-j. Xia, F. H. Zhou, T.-h. Wang, X.-y. Wang, Intrathecal injection of lentivirus-mediated glial cell line–derived neurotrophic factor RNA interference relieves bone cancer-induced pain in rats. *Cancer Sci.* **106**, 430–437 (2015).

35. M. Kanao, H. Kanda, W. Huang, S. Liu, H. Yi, K. A. Candiotti, D. A. Lubarsky, R. C. Levitt, S. Hao, Gene transfer of glutamic acid decarboxylase 67 by herpes simplex virus vectors suppresses neuropathic pain induced by human immunodeficiency virus gp120 combined with ddC in rats. *Anesth. Analg.* **120**, 1394–1404 (2015).

36. B. Storek, M. Reinhardt, C. Wang, W. G. M. Janssen, N. M. Harder, M. S. Banck, J. H. Morrison, A. S. Beutler, Sensory neuron targeting by self-complementary AAV8 via lumbar puncture for chronic pain. *Proc. Natl. Acad. Sci. U.S.A.* **105**, 1055–1060 (2008).

37. L. Fan, X. Guan, W. Wang, J.-Y. Zhao, H. Zhang, V. Tiwari, P. N. Hoffman, M. Li, Y.-X. Tao, Impaired neuropathic pain and preserved acute pain in rats overexpressing voltage-gated potassium channel subunit Kv1.2 in primary afferent neurons. *Mol. Pain* **10**, 8 (2014).

38. J. Braz, C. Beaufour, A. Coutaux, A. L. Epstein, F. Cesselin, M. Hamon, M. Pohl, Therapeutic efficacy in experimental polyarthritis of viral-driven enkephalin overproduction in sensory neurons. *J. Neurosci.* **21**, 7881–7888 (2001).

39. K. Quick, J. Zhao, N. Eijkelkamp, J. E. Linley, F. Rugiero, J. J. Cox, R. Raouf, M. Gringhuis, J. E. Sexton, J. Abramowitz, R. Taylor, A. Forge, J. Ashmore, N. Kirkwood, C. J. Kros, G. P. Richardson, M. Freichel, V. Flockerzi, L. Birnbaumer, J. N. Wood, TRPC3 and TRPC6 are essential for normal mechanotransduction in subsets of sensory neurons and cochlear hair cells. *Open Biol.* **2**, 120068 (2012).

40. D. Vilceanu, C. L. Stucky, TRPA1 mediates mechanical currents in the plasma membrane of mouse sensory neurons. *PLOS ONE* **5**, e12177 (2010).

41. T. Foulkes, M. A. Nassar, T. Lane, E. A. Matthews, M. D. Baker, V. Gerke, K. Okuse, A. H. Dickenson, J. N. Wood, Deletion of annexin 2 light chain p11 in nociceptors causes deficits in somatosensory coding and pain behavior. *J. Neurosci.* **26**, 10499–10507 (2006).

42. T. E. Hawkins, J. Roes, D. Rees, J. Monkhouse, S. E. Moss, Immunological development and cardiovascular function are normal in annexin VI null mutant mice. *Mol. Cell. Biol.* **19**, 8028–8032 (1999).

43. L. Vulchanova, D. J. Schuster, L. R. Belur, M. S. Riedl, K. M. Podetz-Pedersen, K. F. Kitto, G. L. Wilcox, R. S. McIvor, C. A. Fairbanks, Differential adeno-associated virus mediated gene transfer to sensory neurons following intrathecal delivery by direct lumbar puncture. *Mol. Pain* **6**, 31 (2010).

44. T. Pitcher, J. Sousa-Valente, M. Malcangio, The monoiodoacetate model of osteoarthritis pain in the mouse. *J. Vis. Exp.* **2016**, 53746 (2016).

45. R. Linden, chap. PCT/EP2015/053335 (2015).

46. E. I. Takesue, W. Schaefer, E. Jukniewicz, Modification of the Randall-Selitto analgesic apparatus. *J. Pharm. Pharmacol.* **21**, 788–789 (1969).

Science Signaling

Inhibition of somatosensory mechanotransduction by annexin A6

Ramin Raouf, Stéphane Lolignier, Jane E. Sexton, Queensta Millet, Sonia Santana-Varela, Anna Biller, Alice M. Fuller, Vanessa Pereira, Jyoti S. Choudhary, Mark O. Collins, Stephen E. Moss, Richard Lewis, Julie Tordo, Els Henckaerts, Michael Linden and John N. Wood

A blocker of osteoarthritic pain

Patients with osteoarthritis experience pain when moving or, sometimes, touching the affected joints. Raouf *et al.* identified proteins that bound to a toxin that inhibits mechanically induced pain, including the membrane-binding protein annexin A6. Mice lacking annexin A6 were more sensitive to mechanically induced pain, whereas overexpression of annexin A6 in sensory neurons reduced pain in a mouse model of osteoarthritis. These results suggest that strategies that increase the abundance of annexin A6 could alleviate the chronic pain of osteoarthritis.

ARTICLE TOOLS	http://stke.sciencemag.org/content/11/535/eaao2060
SUPPLEMENTARY MATERIALS	http://stke.sciencemag.org/content/suppl/2018/06/15/11.535.eaao2060.DC1
RELATED CONTENT	http://stke.sciencemag.org/content/sigtrans/9/440/ra79.full http://science.sciencemag.org/content/sci/356/6343/1168.full http://stm.sciencemag.org/content/scitransmed/10/428/eaan0746.full http://stke.sciencemag.org/content/sigtrans/11/545/eaao4425.full http://stke.sciencemag.org/content/sigtrans/13/648/eabe6352.full
REFERENCES	This article cites 45 articles, 11 of which you can access for free http://stke.sciencemag.org/content/11/535/eaao2060#BIBL
PERMISSIONS	http://www.sciencemag.org/help/reprints-and-permissions

Use of this article is subject to the Terms of Service